Chaotic wavefield gradiometry

Sjoerd de Ridder and Biondo Biondi

ABSTRACT

We propose a new technique for passive seismic imaging via the direct application of operators to noise recordings. We propose a time-domain 2D scalar wave equation to describe the propagation of surface waves within a narrow frequency range. Outside the source region, this scalar wave equation relates the second-order spatial and second-order temporal derivatives of the wavefield with the local velocity. Different from seismic interferometry, this technique does not rely on cross-correlations to reveal the statistical coherence of a chaotic wavefield at two locations. Rather, it relies on the local measurements of velocity obtained directly from the ratio between temporal and spatial derivatives of the wavefield. The new method allows us to do passive imaging with much shorter passive recordings. Numerical data examples show that this theory can yield reliable images if the wavefield is sampled sufficiently in space and time.

INTRODUCTION

Geophysicists have long attempted to image chaotic wavefields. Aki (1957) first derived the dispersion of surface waves from the cross-correlations of a circle of stations. Claerbout (1968) showed that the one dimensional auto-correlation of transmission responses would yield the reflection response and later conjectured an extension to three-dimensions by cross-correlations. See Wapenaar et al. (2008) for a good review of seismic interferometry. Almost all approaches have centered on correlating long ambient seismic recordings made at two stations. Seismic interferometry has found its most wide application in the retrieval of surface waves (Campillo and Paul, 2003; Shapiro and Campillo, 2004; Shapiro et al., 2005; Gerstoft et al., 2006; Yao et al., 2006; Lin et al., 2008).

However, the advent of ever larger and denser arrays covering the earth's surface provides a complete recording of the surface-wave wavefield not aliased in either time or space in many regions and frequency bands of interest. This essentially entails a direct measurement of local medium properties because the temporal and spatial derivatives of the wavefield are related by the medium properties through the wave equation. Here we exploit this relationship by the development of a wavefield gradiometry method that can be directly applied to chaotic (and non-chaotic) scalar wavefields.

Using wavefield gradients to infer propagation velocity is not a new concept. Using the gradients of the wavefield gradiometry to extract the velocity field has been proposed by Langston (2007a,c,b). The first-order spatial and temporal derivatives of the wavefield amplitudes can be inverted for a set of wavefield coefficients, which relate to the local ray parameter, local wave directionality, local geometrical spreading and local radiation pattern. This technique was applied on recordings of the Embayment Seismic Excitation Experiment in a one-dimensional linear array (Langston, 2007a,b), in two dimensions using local earthquakes recorded by a small array near Moscow Tennessee (Langston, 2007c) and on several earthquakes recorded by US Array (Liang and Langston, 2009).

The fundamental assumption of this work is that the wavefield at each point consists of non-overlapping propagating plane waves from a point source (Langston, 2007a,c). This assumption limits the use of wavefield gradiometry to deterministic wavefields where specific arrivals can be identified. However, here we pose a two-dimensional scalar wave equation for the propagation of a chaotic wavefield consisting of single mode surface waves. We devise a strategy for chaotic wavefield gradiometry based on second-order partial derivatives of the observed chaotic wavefield amplitudes.

In this paper we first develop the method as a discrete computation for wavefields densely and irregularly sampled in space and regularly in time. Then I provide several numerical examples using both an analytic and finite-difference solution to the two-dimensional scalar wave equation.

CHAOTIC WAVEFIELD GRADIOMETRY

We assume that surface wave propagation in two dimensions is governed by a two-dimensional scalar wave equation for each frequency component of the wavefield:

$$\mathrm{c}^2(x,\omega)\nabla^2\hat{\mathrm{u}}(x,\omega) + \omega^2\hat{\mathrm{u}}(x,\omega) = -\hat{\mathrm{s}}(x,\omega), \tag{1}$$

where u is the wavefield variable observable in time and space and $\hat{\mathrm{u}}$ its Fourier transformed counterpart, s is a generalized source term and $\hat{\mathrm{s}}$ its Fourier transformed counterpart, ∇^2 is the Laplacian acting on the spatial dimensions and c is the phase velocity. After a sufficiently narrow bandpass filter (with central frequency ω'), for frequencies over which we can neglect the frequency dependence of the phase velocity, the filtered wavefield obeys:

$$\mathrm{c}^2_{\omega'}(x)\nabla^2\mathrm{u}(x,t) - \partial_t^2\mathrm{u}(x,t) = -\mathrm{s}(x,t), \tag{2}$$

where ∂_t^2 is the second-order derivative acting on the time dimension and $\mathrm{c}_{\omega'}$ is the phase velocity for this central frequency.

For chaotic wavefields the source distribution is generally unknown. Unless local sources dominate, we can assume that the source distribution is zero within the area of recordings:

$$\nabla^2\mathrm{u}(x,t)\ \mathrm{c}^2_{\omega'}(x) = \partial_t^2\mathrm{u}(x,t). \tag{3}$$

If sufficiently dense recordings are available we can evaluate the spatial and temporal second-order derivatives by finite differences. Let $\mathbf{u}(\mathbf{x},\mathbf{t})$ denote the discrete recordings of the wavefield, and $\mathbf{D_{tt}}$ and $\mathbf{D_{xx}}$ are (usually sparse) matrices containing finite-difference approximations of the second-order derivative operators applied to the wavefield in time and space, respectively. Then for each time slice $\mathbf{u}_i = \mathbf{u}(\mathbf{x}, t_i)$ equation 3 can be written as:

$$\mathbf{W}\mathrm{diag}\left\{\mathbf{D_{xx}}\mathbf{u}_i\right\}\ \mathbf{c}^2_{\omega'}(\mathbf{x}) = \mathbf{W}\mathbf{D_{tt}}\mathbf{u}_i, \tag{4}$$

where $\mathbf{D_t}$ operates on a few adjacent time slices, diag$\{\ \}$ denotes a diagonal operator specifying the elements on the diagonal between $\{\ \}$. We can discard locations with poor measurements using a masking operator, $\mathbf{W}$, which has the structure of a diagonal matrix with ones and zeros on the diagonal elements. Equation 4 has the structure $\mathbf{F}_i\,\mathbf{m} = \mathbf{b}_i$, where $\mathbf{m} = \mathbf{c}^2_{\omega'}(\mathbf{x})$, $\mathbf{F}_i = \mathrm{diag}\left\{\mathbf{D_{xx}}\mathbf{u}_i\right\}$, and $\mathbf{b}_i = \mathbf{D_{tt}}\mathbf{u}_i$. We form these data fitting equations for a set of $\mathrm{N_t}$ time slices in the data, and the least-squares estimator for $\mathbf{m}$ is given by inverting:

$$\sum_{i=1}^{N_t} \mathbf{F}_i^\dagger \mathbf{W}^\dagger \mathbf{W} \mathbf{F}_i\ \mathbf{m} = \sum_{i=1}^{N_t} \mathbf{F}_i^\dagger \mathbf{W}^\dagger \mathbf{W} \mathbf{b}_i, \tag{5}$$

where $\dagger$ denotes matrix adjoint. The solution for each element of $\mathbf{m}(\mathbf{x})$ is essentially an independent division of the second-order temporal derivative of the wavefield by the second-order spatial derivative of the wavefield. This ratio is evaluated at each point in space and averaged over all recording time by linear regression. We implicitly assume that the velocity does not change significantly across the length of the spatial finite-difference stencil.

We wish to add a spatial smoothness constraint on $\mathbf{m}$ by adding the spatial smoothness regularization $\epsilon\nabla^2\mathbf{m} = \mathbf{0}$, where ϵ determines the importance of the model-styling goal versus the data-fitting equations. To aid the inversion, we decompose $\mathbf{m}$ into a background and a perturbation, $\mathbf{m} = \mathbf{m}_0 + \Delta\mathbf{m}$. This Laplacian is evaluated using the same finite-difference approximation $\mathbf{D_x}$ as before. The least-squares estimator for $\Delta\mathbf{m}$ is given by inverting:

$$\begin{aligned}\left[\sum_{i=1}^{N_t} \mathbf{F}_i^\dagger \mathbf{W}^\dagger \mathbf{W} \mathbf{F}_i + \epsilon^2 \mathbf{D}_{\mathbf{xx}}^\dagger \mathbf{D_{xx}}\right] \Delta\mathbf{m} = \\ \sum_{i=1}^{N_t} \mathbf{F}_i^\dagger \mathbf{W}^\dagger \mathbf{W} \mathbf{b}_i - \left[\sum_{i=1}^{N_t} \mathbf{F}_i^\dagger \mathbf{W}^\dagger \mathbf{W} \mathbf{F}_i + \epsilon^2 \mathbf{D}_{\mathbf{xx}}^\dagger \mathbf{D_{xx}}\right] \mathbf{m}_0.\end{aligned} \tag{6}$$

We choose $\mathbf{m}_0$ to be a scalar and an estimate for the background model obtained from the ratio between the second-order temporal derivative and second-order spatial derivative averaged over all time and all points in space:

$$\mathrm{m}_0 = \frac{1}{X}\sum_{j=1}^{N_s} \mathrm{diag}\left\{\sum_{i=1}^{N_t} \mathbf{F}_i^\dagger \mathbf{W}^\dagger \mathbf{W} \mathbf{b}_i\right\}_j^{-1} \mathrm{diag}\left\{\sum_{i=1}^{N_t} \mathbf{F}_i^\dagger \mathbf{W}^\dagger \mathbf{W} \mathbf{F}_i\right\}_j, \tag{7}$$

where j is the index over the elements of the diagonals, N_s is the total number of stations, and X is the cardinality of the set in the masking matrix, $\mathbf{W}$. Because $\mathbf{m}_0 = \mathrm{m}_0$ is a constant over space, its spatial second-order derivative vanishes, and equation 6 reduces to:

$$\left[\sum_{i=1}^{N_t} \mathbf{F}_i^\dagger \mathbf{W}^\dagger \mathbf{W} \mathbf{F}_i + \epsilon^2 \mathbf{D}_{\mathbf{xx}}^\dagger \mathbf{D}_{\mathbf{xx}}\right] \Delta\mathbf{m} = \sum_{i=1}^{N_t} \mathbf{F}_i^\dagger \mathbf{W}^\dagger \mathbf{W} \mathbf{b}_i - \sum_{i=1}^{N_t} \mathbf{F}_i^\dagger \mathbf{W}^\dagger \mathbf{W} \mathbf{F}_i \; \mathbf{m}_0. \qquad (8)$$

Finally we retrieve the phase velocity, $c(x)$, from the inverted model perturbation using $c(x) = \sqrt{\mathrm{m}_0 + \Delta\mathrm{m}(x)}$. This method for imaging a chaotic wavefield does not employ cross-correlations.

NUMERICAL DATA EXAMPLES

We test the method presented in the previous section on three synthetic models: The first model is a homogeneous medium with velocity 2000 m/s. The second model is a Gaussian anomaly of 50 m/s on a homogeneous background medium with velocity 2000 m/s. The third model is a two layer medium with 1950 m/s and 2050 m/s. We consider three source distributions: The first distribution is one source in the center of the domain. The second distribution consists of two sources at either side of the center of the domain. The third distribution consists of a large number of sources acting randomly in time, and positioned randomly on a boundary outside the domain. The matrices $\mathbf{D_{tt}}$ and $\mathbf{D_{xx}}$ contain second order finite-difference approximations to the second order spatial and temporal derivatives.

For the first set of examples, I use a far-field analytic solution in a homogeneous medium. I compute the wavefield radiating from a source located in the center of the medium. The wavefield is computed at a spacing of 0.5 m and with a sampling of 0.25 ms for a Ricker wavelet with central frequency of 75 Hz as the source. Because there is no noise or error, we omit the spatial smoothness regularization. The recovered velocity models for the three source distributions in a homogeneous medium are shown in Figure 1. Figure 2 shows profiles through the true and recovered homogeneous velocity models. The dashed lines in Figure 1 correspond to the locations of the profiles of Figure 2. Figures 1a-b and 2a-b reveal that the recovered velocity is very wrong near the sources. This is because the Green's solution used to model the wavefield is only a far-field solution and not a full solution to equation 2. When the sources are placed outside the domain to be imaged, we retrieve the correct velocity profile (Figure 2c). We computed the wavefield with very small temporal and spatial sampling intervals, so the error in the finite-difference approximation of the derivative operators is small. However, there is still a small discrepancy between the true and recovered velocities. This is due to the small remaining error in the finite-difference coefficients.

The second set of examples is made using wavefields computed using finite differences (4th order in time and 16th order in space). For the three models and the

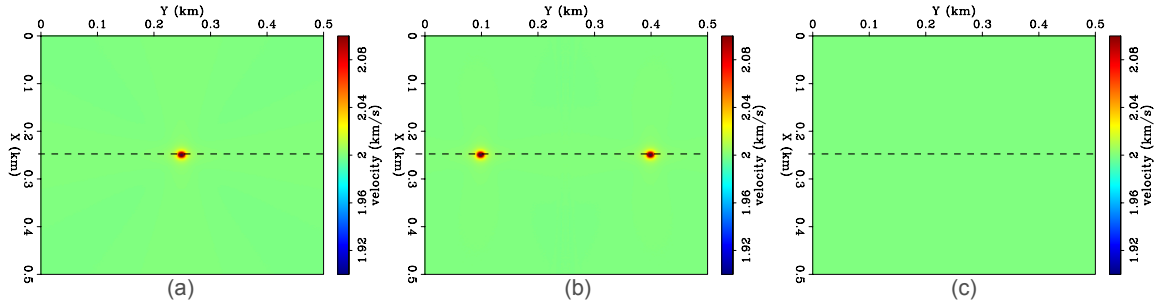

Figure 1: Recovered velocity models using an analytic solution to the wave equation in a homogeneous medium. a) Singe source at the center; b) Two sources on either side of the center; c) Sources placed randomly at the boundaries. Dashed lines indicate the locations of the profiles in Figure 2. [**ER**]

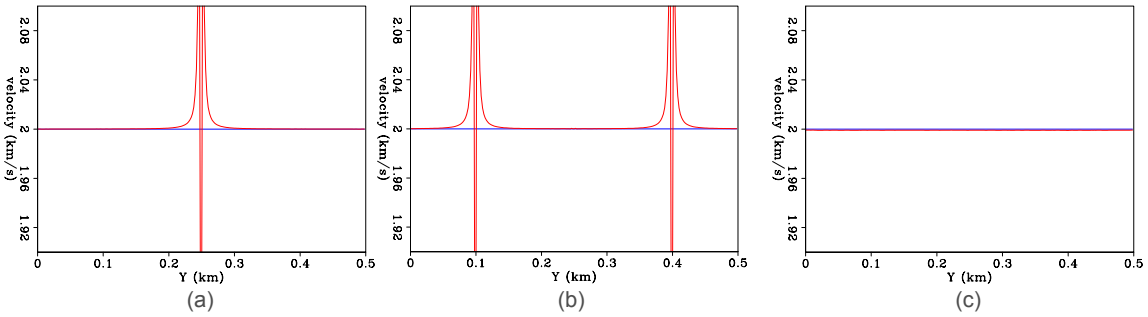

Figure 2: Profiles through true (blue) and recovered (red) homogeneous velocity models using an analytical solution to the wave equation in a: a) Single source at the center; b) Two sources on either side of the center; c) Sources placed randomly at the boundaries. [**ER**]

three source distributions, the wavefields are computed at a spacing of 0.5 m and with a sampling of 0.25 ms for a Ricker wavelet with central frequency of 75 Hz as the source. For all three models and three source distributions the recovered models are shown in Figure 3. Profiles through true and recovered velocity models are shown in Figure 4. The dashed lines in Figure 3 correspond to the locations of the profiles of Figure 4. There is no large discrepancy between true and recovered velocity model in the vicinity of the sources. This is because the finite-difference modeling code includes both far-field and near-field terms of the solution to the wave equation. The distinct flower-like pattern centered around the source is due to the anisotropic error of the finite difference stencils in both the modeling step and the wavefield gradiometry step. One profile of recovered velocities in Figure 4 deviates significantly from the true velocity model (Figure 4h). This profile is taken exactly at a point in space where the wavefields from both sources interfere in time and the effective spatial wavelength becomes shorter. One explanation of the increased error may be that the error of the finite-difference stencil becomes significant.

In principle the method has no difficulty retrieving smooth or sharp velocity contrasts. However in practice, the resolution of the method cannot supersede the spatial sampling of the wavefield by the array. Furthermore, the resolution of chaotic wavefield gradiometry will depend on the length of the stencils used to evaluate the finite-difference approximations of the operators.

CONCLUSIONS

We presented a new method to extract surface-wave phase velocities from ambient seismic recordings: chaotic wavefield gradiometry. The method is based on evaluating the second-order spatial and temporal derivatives in the two-dimensional scalar wave equation to directly infer phase velocities. In contrast with conventional methods to image chaotic ambient seismic noise, this method does not employ cross-correlations. Numerical data examples show that the method would work well if the wavefield is recorded sufficiently in space and time. The retrieved velocity is very sensitive to the error in the approximations of the operators by the finite differences. The recovery of sharp velocity contrasts depends on sampling the wavefield very densely.

ACKNOWLEDGMENTS

We thank Joseph Stefani, Dimitri Bevc and Mark Meadows from Chevron's Center of Research Excellence (CORE) at Stanford and Gustavo Alves, Ohad Barack, Jason Chang, Bob Clapp, Jon Claerbout, Taylor Dahlke, Stew Levin, Musa Maharramov, Eileen Martin and Mandy Wong from the Stanford Exploration Project for helpful discussions and suggestions. Sjoerd de Ridder thanks Chevron's CORE at Stanford for supporting his visit to Stanford University during July and August of 2014.

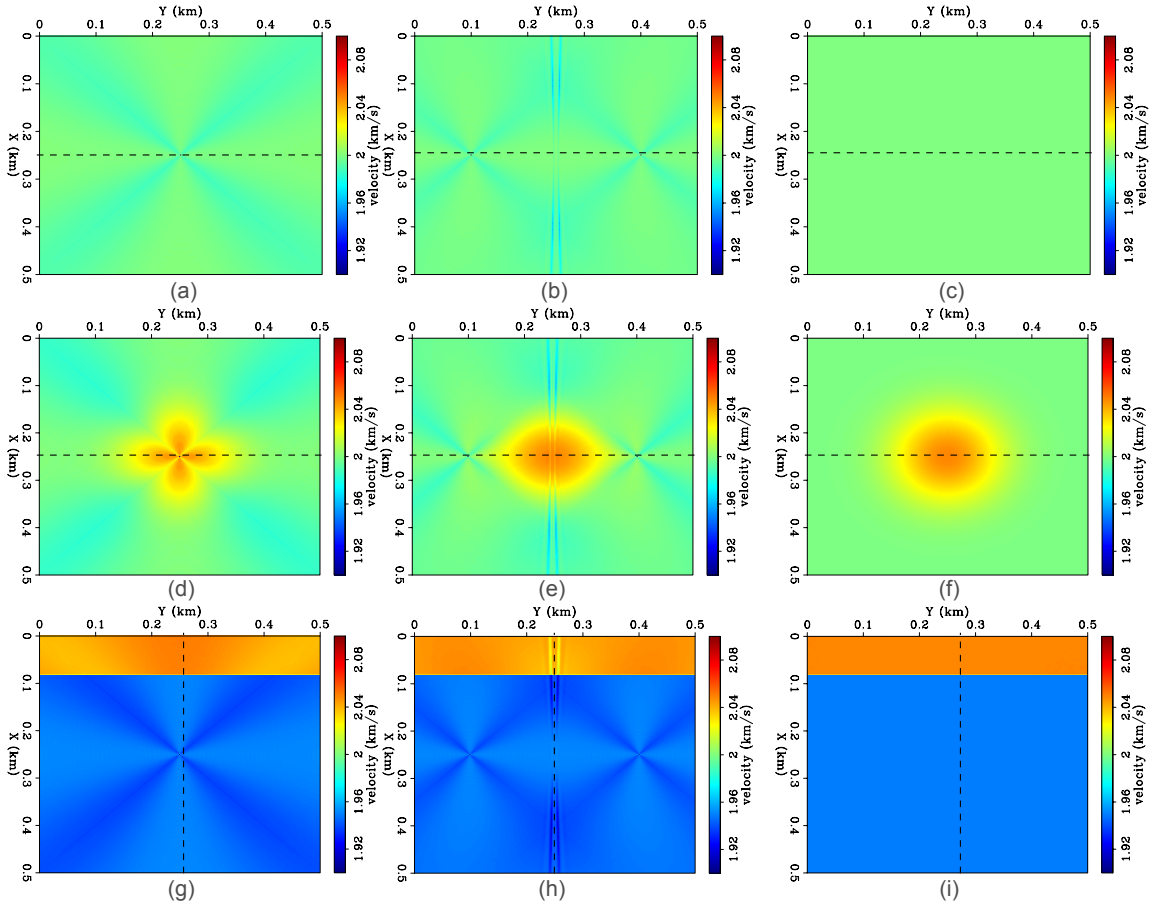

Figure 3: Recovered velocity models using finite difference solutions to the wave equation in: a-c) A homogeneous velocity model; d-f) A Gaussian anomaly; g-i) A two layer medium. Source distributions for the wavefields: a,d,g) Singe source at the center; b,e,h) Two sources on either side of the center; c,f,i) Sources placed randomly at the boundaries. Dashed lines indicate the locations of the profiles in Figure 4. [**ER**]

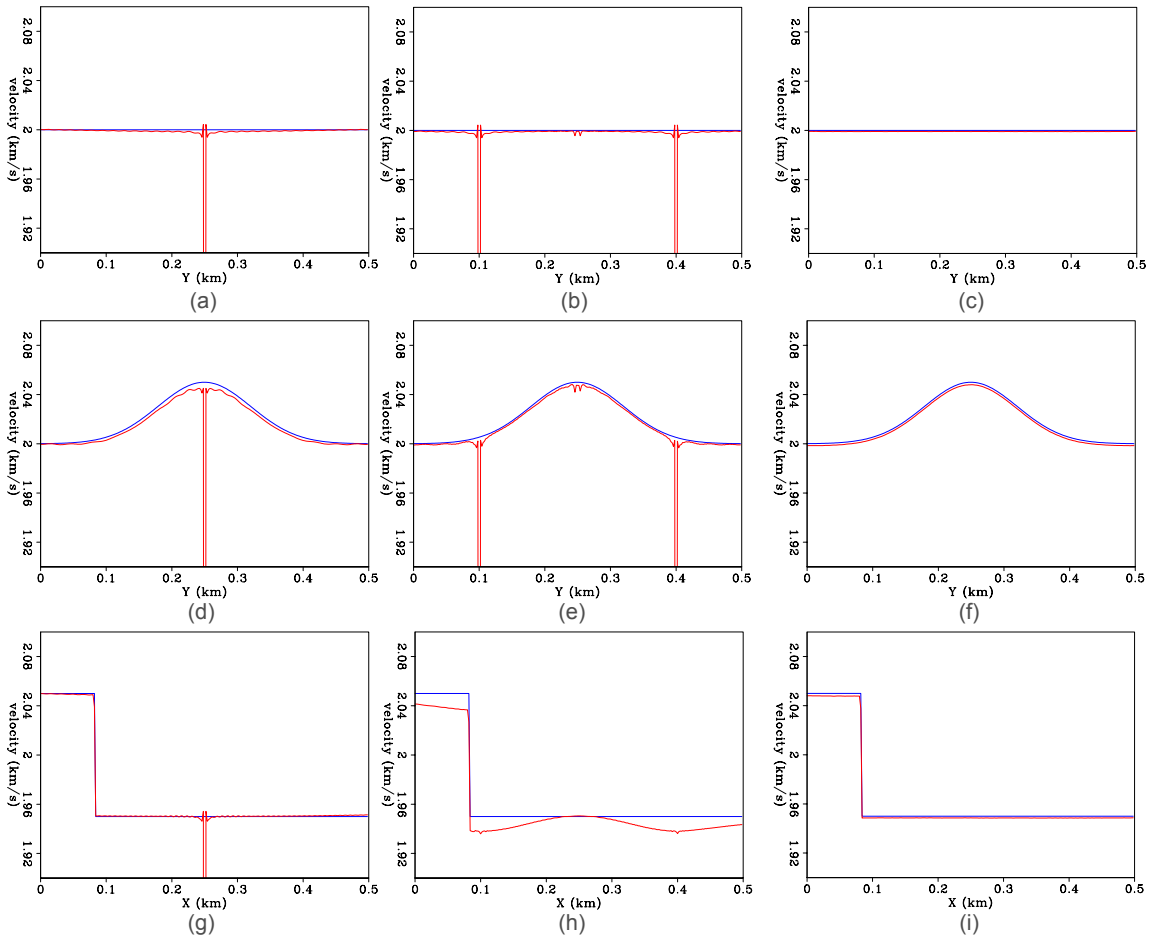

Figure 4: Profiles through true (blue) and recovered (red) velocity models using finite difference solutions to the wave equation in: a-c) A homogeneous velocity model; d-f) A Gaussian anomaly; g-i) A two layer medium. Source distributions for the wavefields: a,d,g) Singe source at the center; b,e,h) Two sources on either side of the center; c,f,i) Sources placed randomly at the boundaries. [**ER**]

REFERENCES

Aki, K., 1957, Space and time spectra of stationary stochastic waves, with special reference to microtremors: Bulletin of the Earthquake Research Institute, **35**, 415–456.

Campillo, M., and A. Paul, 2003, Long-range correlations in the diffuse seismic coda: Science, **299**, 547–549.

Claerbout, J. F., 1968, Synthesis of a layered medium from its acoustic transmission response: Geophysics, **33**, 264–269.

Gerstoft, P., K. G. Sabra, P. Roux, W. A. Kuperman, and M. C. Fehler, 2006, Green's functions extraction and surface-wave tomography from microseisms in southern California: Geophysics, **71**, no. 4, SI23–SI31.

Langston, C. A., 2007a, Spatial gradient analysis for linear seismic arrays: Bulletin of the Seismological Society of America, **97**, 265–280.

———, 2007b, Wave gradiometry in the time domain: Bulletin of the Seismological Society of America, **97**, 926–933.

———, 2007c, Wave gradiometry in two dimensions: Bulletin of the Seismological Society of America, **97**, 401–416.

Liang, C., and C. A. Langston, 2009, Wave gradiometry for usarray: Rayleigh waves: Journal of Geophysical Research: Solid Earth, **114**, n/a–n/a.

Lin, F.-C., M. P. Moschetti, and M. H. Ritzwoller, 2008, Surface wave tomography of the western united states from ambient seismic noise: Rayleigh and love wave phase velocity maps: Geophysical Journal International, **173**, 281–298.

Shapiro, N. M., and M. Campillo, 2004, Emergence of broadband Rayleigh waves from correlations of the ambient seismic noise: Geophysical Research Letters, **31**, L07614–1–L07614–4.

Shapiro, N. M., M. Campillo, L. Stehly, and M. H. Ritzwoller, 2005, High-resolution surface-wave tomography from ambient seismic noise: Science, **307**, 1615–1618.

Wapenaar, K., D. Draganov, and J. Robertsson, 2008, Seismic interferometry: History and present status: Society of exploration geophysicists, geophysics reprint series no. 26: Society of Exploration Geophysicists.

Yao, H., R. D. Van Der Hilst, and M. V. De Hoop, 2006, Surface-wave array tomography in SE Tibet from ambient seismic noise and two-station analysis - I. Phase velocity maps: Geophysical Journal International, **166**, 732–744.